Chapter 17

Kinetic Modeling of Plant Metabolism and Its Predictive Power: Peppermint Essential Oil Biosynthesis as an Example

Bernd Markus Lange and Rigoberto Rios-Estepa

Abstract

The integration of mathematical modeling with analytical experimentation in an iterative fashion is a powerful approach to advance our understanding of the architecture and regulation of metabolic networks. Ultimately, such knowledge is highly valuable to support efforts aimed at modulating flux through target pathways by molecular breeding and/or metabolic engineering. In this article we describe a kinetic mathematical model of peppermint essential oil biosynthesis, a pathway that has been studied extensively for more than two decades. Modeling assumptions and approximations are described in detail. We provide step-by-step instructions on how to run simulations of dynamic changes in pathway metabolites concentrations.

Key words Deterministic, Essential oil, Kinetic, Modeling, Monoterpene, Peppermint, Stochastic

1 Introduction

Microbial cells grown under controlled conditions can reach a *dynamic equilibrium*, or metabolic *steady-state*, when nutrients are derived from the medium and metabolic end products are accumulated or excreted at constant rates. This means that the concentrations of all metabolic intermediates remain constant because their rates of formation are balanced with their rates of degradation. For this to occur there needs to be a constant flux of matter through the metabolic pathways. A simple example of such a system is a bathtub with an open tap but without a bottom plug. After a certain time the water flows in and out at the same rate, so the water level stabilizes and the system is at steady state. Obviously, a metabolic steady-state is a mathematical abstraction but, if metabolism is only subjected to relatively small and slow changes, pathways may still be regarded as being in *quasi steady-state*. These approximations have allowed the development of various mathematical approaches to model cellular metabolism. However, although quasi steady-state

Ganesh Sriram (ed.), *Plant Metabolism: Methods and Protocols*, Methods in Molecular Biology, vol. 1083, DOI 10.1007/978-1-62703-661-0_17,

conditions can be attained in plant cells under artificial growth conditions, metabolism in plants grown under realistic environmental conditions is controlled by numerous factors that generate non-steady-state conditions. At the cellular level plant cells have multiple compartments that impede a free flux of metabolites and build up energy gradients across their membranes. At the plant tissue and organ level, cell-type specialization plays an important role and constrains metabolic flows. At the whole plant level, large parts of metabolism oscillate dynamically according to the circadian rhythm of the intrinsic clock. Plants are responsive to environmental cues, which may be of both biotic (e.g., pathogens, insects, and herbivores) and abiotic (e.g., light, temperature, and nutrition) nature. In summary, these examples illustrate limitations of static modeling approaches. To capture the adaptations of plant metabolism to changes in experimental or field growth conditions, it is thus highly desirable to employ dynamic models. So what does it take to develop such a dynamic (kinetic) mathematic model?

The *first consideration* is the size or scope of the model. Is the main interest a single pathway or a network of pathways at the cellular, tissue, organ, or even whole plant level? This decision has to be guided by the existing knowledge with regard to network architecture (the "parts list" of enzymes and metabolites), the properties of the individual network entities (enzyme kinetics), flux distribution (how much carbon is channeled into different pathway branches under different conditions), and barriers (e.g., transport of metabolites across membranes). Although the most ambitious projects are aimed at generating kinetic models of whole cell metabolism [1], true advances in our understanding of pathway control have come from studies of smaller, clearly defined, subnetworks (reviewed in ref. 2).

The *second consideration* relates to the modeling approach. There are two fundamentally different paths:

1. In *deterministic modeling* one assumes that the future of an experimental system is completely determined by its present and past. In deterministic kinetic models the system of study is seen as a homogeneous medium with random interactions among reactants (enzymes and metabolites). This approach generally works well when overall flux is determined primarily at the level of enzyme properties.
2. When fluctuations of biomolecules are large or to a certain extent erratic, which is often the case when transcriptional regulation of gene expression is included in models [3], a *stochastic modeling* approach is more appropriate. A stochastic process evolves over time and probability distributions of potential outcomes are obtained by allowing for random variation in one or more inputs (e.g., gene expression levels) over time. The random variation is usually based on fluctuations observed

in experimental data for a specific time period. Distributions of potential outcomes are derived from a large number of simulations (stochastic projections) that reflect the random variation in the input(s), and a model of an entire pathway or even a larger network of pathways thus requires substantial computational resources.

The *third consideration* for modeling is the source of modeling parameters. In some cases it might be appropriate to take enzyme kinetic data from the published literature, while caution needs to be exerted when using kinetic constants determined by in vitro assays [4].

The *fourth consideration* pertains to the estimation of parameters for which experimental measurements are not available [5]. There might be a series of steps that can be treated collectively as a "black box", which is appreciated solely in terms of its input, output and transfer characteristics, without any knowledge of its internal workings. Certain parameters can potentially be estimated by an iterative process of estimating values and determining the fit of model simulations with experimental measurements.

The *fifth consideration* concerns the validation of the model by comparing the biochemical results predicted from the kinetic data with those measured directly by chemometric means [6]. Statistical methods that consider the goodness of fit should be used to guide the selection among alternative models.

2 Materials

The experimental protocols for growing plants and determining the parameters and variables of an example kinetic mathematical model have been described in detail elsewhere [7, 8]. We recommend using MATLAB® version 7.11 or later (Mathworks, Natick, MA, USA) on a personal computer with at least 3 GB of available disk space and at least 1,024 MB of random access memory. However, the scripts listed in this article will also run on earlier MATLAB versions.

3 Methods

In this paragraph we outline—step-by-step—the process of developing a deterministic kinetic model. We use the peppermint monoterpenoid essential oil pathway as an example because, in distinction to many other currently available kinetic models, most modeling assumptions are supported directly by experimental data, and the quality of simulations of monoterpene profiles can thus be employed to assess our understanding of pathway structure and regulation [7, 8]. Peppermint monoterpene biosynthesis is a

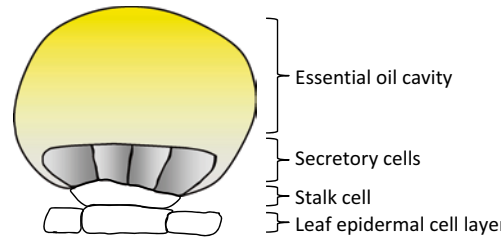

Fig. 1 Depiction of a cross section of a peppermint leaf glandular trichome. The secretory cell disk, which harbors the biosynthetic machinery for essential oil biosynthesis, is colored in *gray*. The essential oil stored within a subcuticular storage cavity is colored in *yellow* in the online version of this chapter (Color figure online)

complex and highly dynamic process. We will describe how modeling variables and parameters are derived by starting with macroscopic measurements and how those relate to processes operating at microscopic and molecular scales.

3.1 Anatomical Specialization of Peppermint Monoterpene Biosynthesis

The synthesis and accumulation of monoterpenoid essential oils in peppermint (and other members of the mint family) is restricted to specialized anatomical structures called glandular trichomes (reviewed in ref. 9) (Fig. 1). More specifically, the enzymatic machinery for monoterpene biosynthesis (Fig. 2) is only present in the eight secretory cells that form a disk-like structure situated on top of a single stalk cell (colored in gray in Fig. 1). The essential oil is accumulated in a preformed subcuticular storage cavity of the glandular trichome (colored in yellow in Fig. 1 in the online version of this chapter).

3.1.1 Estimating the Essential Oil Production of Individual Glandular Trichomes

The quantification of peppermint essential oil is generally performed by hydrodistillation and subsequent gas chromatographic analysis of the oil collected thereby [10]. In order to model monoterpene biosynthesis at the cellular level it is necessary to calculate the amount of oil synthesized by an individual glandular trichome. We employed two independent approaches to estimate the oil volume per glandular trichome by:

1. Counting the average number of glandular trichomes on a mature peppermint leaf and dividing the total average oil yield per mature leaf by this number.
2. Estimating the average dimensions of the oil-containing cavity of a glandular trichome based on microscopic images [7, 8].

Both approaches gave similar results. For modeling purposes we used an oil volume of 2.03×10^{-4} µl for mature (large-sized) trichomes. Peppermint leaves contain a distribution of glandular trichomes of different sizes, which depends on leaf age and growth conditions [11]. For more accurate calculations of oil volumes we

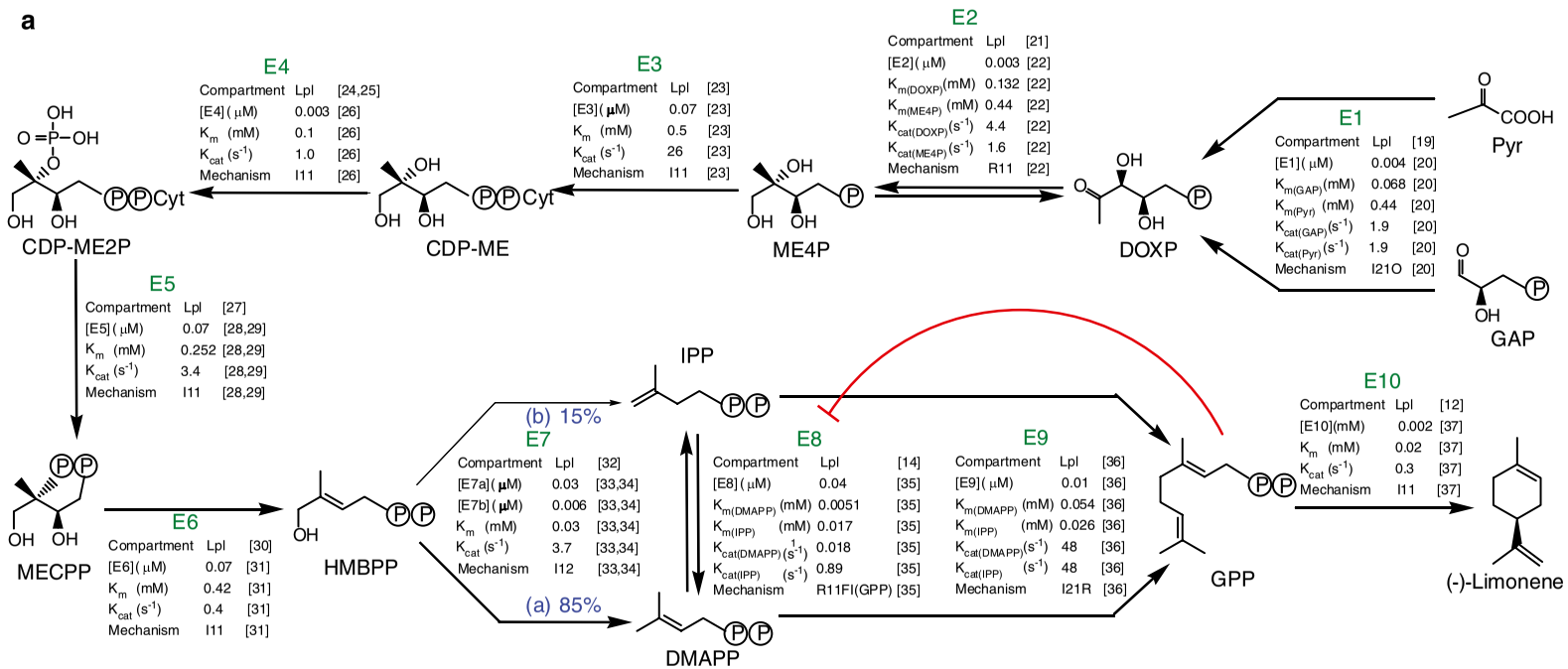

Fig. 2 Outline of peppermint monoterpenoid essential oil biosynthesis. The figure is split into two parts: (**a**) the precursor supply steps and (**b**) the essential oil-specific steps. The parameters used for modeling are listed for each enzyme, including the appropriate references in *brackets*. Feedback inhibition is indicated by a *red arc* with a *short orthogonal line*. The following enzymes are included in the model: *E1* 1-deoxy-D-xylulose 5-phosphate synthase, *E2* 1-deoxy-D-xylulose 5-phosphate reductoisomerase, *E3* 2C-methyl-D-erythritol 4-phosphate cytidyltransferase, *E4* 4-(cytidine 5′-diphospho)-2C-methyl-D-erythritol kinase, *E5* 2C-methyl-D-erythritol 2,4-cyclodiphosphate synthase, *E6* (E)-4-hydroxy-3-methyl-but-2-enyl diphosphate synthase, *E7* (E)-4-hydroxy-3-methyl-but-2-enyl diphosphate reductase, *E8* isopentenyl diphosphate isomerase, *E9* geranyl diphosphate synthase, E10 (–)-limonene synthase, *E11* (–)-limonene 3-hydroxylase, *E12* (–)-trans-isopiperitenol dehydrogenase, *E13* (–)-trans-isopiperitenone reductase, *E14* (+)-cis-isopulegone isomerase, *E15* (+)-menthofuran synthase, *E16a* (+)-pulegone reductase ((–)-menthone-forming activity), *E16b* (+)-pulegone reductase ((+)-isomenthone-forming activity), *E17a* (–)-menthone: (–)-menthol reductase ((–)-menthol-forming activity), *E17b* (–)-menthone: (–)-menthol reductase ((+)-neoisomenthol-forming activity), *E18a* (–)-menthone: (+)-neomenthol reductase ((+)-neomenthol-forming activity), *E18b* (–)-menthone: (+)-neomenthol reductase ((+)-isomenthol-forming activity). The subcellular compartmentation of enzymes is color-coded in the online version of this chapter: cytosol, *blue*; endoplasmic reticulum, *orange*; leucoplasts, *green*; mitochondria, *red* (Color figure online)

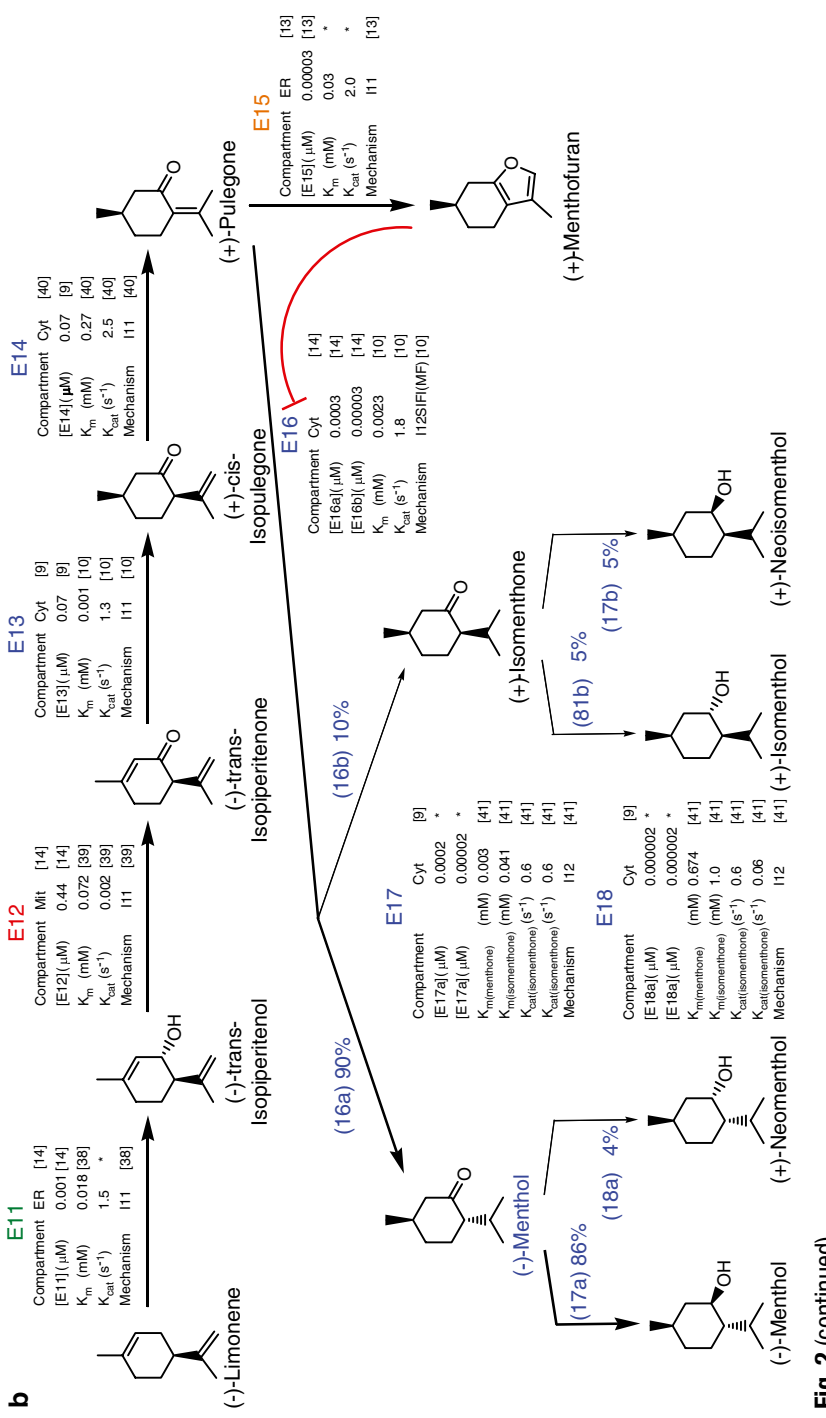

Fig. 2 (continued)

thus included two additional sizes of glandular trichomes: medium-sized (1.40×10^{-4} µl) and small-sized (0.66×10^{-4} µl). Based on microscopic size measurements, leaves of peppermint plants grown under greenhouse conditions contained 39 % large, 57 % medium, and 4 % small glandular trichomes at 30 days after leaf emergence. We counted a total of 10,151 glandular trichomes per leaf, thus indicating a distribution of 3,959 large (39 %), 5786 medium (57 %), and 406 small (4 %) glandular trichomes. The number of glandular trichomes in each size category (e.g., 3,959 large glandular trichomes per leaf) was multiplied by the appropriate trichome volume (e.g., 2.03×10^{-4} µl) to calculate the volume of oil contributed by this glandular trichome category (0.722 µl per leaf). Analogous calculations were performed for mid-sized (731 µl per leaf) and small-sized (24 µl per leaf) glandular trichomes. The known density of peppermint essential oil (0.9) then allowed us to estimate the total essential oil amount (1,535 µg per leaf). Varying oil yields determined with peppermint grown under various experimental conditions or in different peppermint genotypes (transgenics) can thus be correlated with glandular trichome distribution [8].

3.1.2 Consideration of Developmental Trichome Dynamics

A leaf's capacity for essential oil production is dependent on its developmental stage. For a dynamic model of the monoterpene pathway it is thus essential to capture such dynamics in mathematical expressions. It had previously been shown that the density of glandular trichomes correlates directly with leaf age [11]. To simulate these experimentally determined changes in glandular trichome numbers (GN) over time, we introduced a logistic function:

$$GN(t) = \frac{a}{1 + c \times e^{kt}} \quad (1)$$

where: t = time after leaf emergence (variable in the model), a = number of glandular trichomes on a fully expanded leaf (parameter in the model), c = number of times the initial gland population must grow to reach "a" (parameter in the model), and k = factor determining the slope during the growth phase of the curve (parameter in the model).

The parameters a, c and k in Eq. 1 can be varied to adjust for changes in trichome developmental dynamics. For greenhouse-grown plants the best fit between the logistic function and experimental data was achieved with $a = 1$, $c = 8 \times 10^4$, and $k = 1.11 \times 10^{-5}$ (Fig. 3a).

3.2 Subcellular Compartmentation of Biosynthetic Enzymes

The Michaelis–Menten formalism, which is generally used to describe the kinetic behavior of enzymes, requires knowledge of the concentration of the enzyme catalysts. This means that, in order to develop a kinetic model of peppermint essential oil biosynthesis, one must determine or estimate the concentrations of all relevant enzymes in the secretory cells of glandular trichomes.

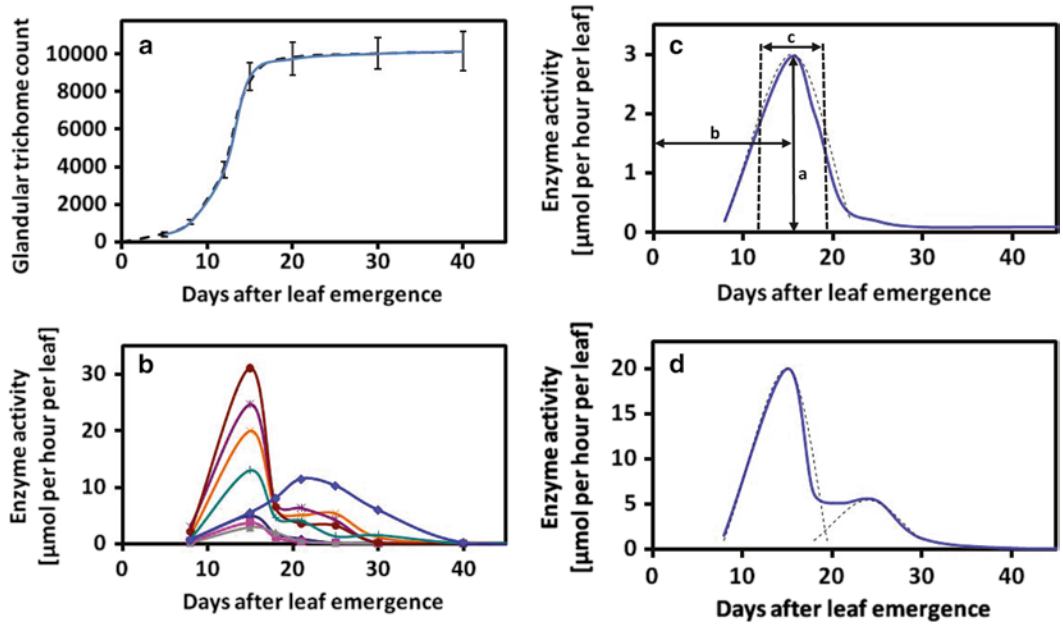

Fig. 3 Approximations of experimentally determined parameters. (**a**) Distribution of glandular trichomes on leaves of wild-type plants grown under greenhouse conditions. The *blue line graph* indicates the experimentally determined number of glandular trichomes for each leaf size class (± standard error). The *broken black line* depicts the logistic function used to approximate glandular trichome numbers (Eq. 1). (**b**) Experimentally determined time courses of enzymes involved in peppermint monoterpene biosynthesis: *maroon circles*, (+)-cis-isopulegone isomerase; *purple* "Y", (–)-Isopiperitenone reductase; *orange* "X", (–)-trans-isopiperitenol dehydrogenase; *green* "+", (+)-pulegone reductase; *blue* "–", (–)-menthone:(–)-menthol reductase; *pink square*, (–)-limonene synthase; *gray triangle*, (–)-limonene 3-hydroxylase. (**c**) Gauss function used to approximate the shape of enzyme activity (Eq. 13); experimental data, *blue line*; Gauss function, *black broken line*. *Lines* are colored in the online version of this chapter. (**d**) Example of the use of two Gauss functions (*broken black lines*) to approximate an enzyme activity curve with two maxima (Color figure online)

Antibodies against most enzymes involved in peppermint monoterpene biosynthesis were available [12–14], which allowed us to use Western blotting to estimate enzyme concentrations in secretory cells isolated from glandular trichomes at peak activity (which for most enzymes is at roughly 15 days after leaf emergence). No experimental data was available regarding the concentrations of enzymes involved in precursor supply pathways, so these values had to be estimated. There was only one more complication: the monoterpene pathway is compartmentalized, which means that biosynthetic enzymes are confined to specific locations within the cell. We used a morphometric approach to estimate the volume densities of organellar compartments in peppermint oil gland secretory cells, which then allowed us to estimate the concentration of each enzyme in the relevant subcellular environment by introducing a compensatory factor ("Comp" in the model). For example, leucoplasts account for

roughly 13.9 % of the area of an actively oil-secreting secretory cell, which means that the "Comp" factor for the adjustment of the concentration of a plastidial enzyme in the model was 0.139. Analogous factors were used for adjusting enzyme concentrations in mitochondria (0.044), the cytosol (0.204), and the membranes of the endoplasmic reticulum (0.365) (Fig. 2).

3.3 In Vitro Kinetics of Enzymatic Reactions

The Michaelis–Menten rate equation, as developed by Briggs and Haldane [15], is a means to calculate the change of the concentration of a metabolite based on the rate of enzymatic formation and turnover. We will now list the appropriate equations for the various enzyme classes involved in the peppermint monoterpene pathway (Fig. 2).

3.3.1 Single Substrate Reactions (Irreversible)

In an irreversible, single-substrate reaction the enzyme (E) first binds the substrate (S) to form an enzyme–substrate complex (ES), before catalyzing a chemical reaction that generates the product (Eq. 2):

$$E + S \rightleftharpoons ES \rightarrow E + P. \tag{2}$$

Assuming that the concentration of ES changes much more slowly than the concentrations of S and P (pseudo steady-state hypothesis), the reaction rate (ν) is obtained as:

$$v = v_{\max} \times \frac{[S]}{K_M} = \frac{K_{cat}}{K_M + [S]} \times [E_0] \times [S] \tag{3}$$

where: $[S]$ = substrate concentration, $\nu_{\max}$ = maximum reaction rate, K_M = Michaelis constant (inverse of enzyme affinity), K_{cat} = turnover number, and $[E_0]$ = enzyme concentration at the beginning of the reaction.

In the context of a metabolic network, the change of a metabolite concentration over time is determined by the rate of formation minus the rate of turnover. For simple, essentially irreversible, reactions the following equation is derived:

$$\frac{dM}{dt} = \nu_{Formation} - \nu_{Consumption}. \tag{4}$$

This approach is appropriate for the following enzymatic reactions of the peppermint monoterpene pathway (identifiers as in Fig. 2): *E3, E4, E5, E6, E10, E11, E12, E13, E14,* and *E15*. The values for K_{cat} and K_m for each enzyme (as shown in Fig. 2) had either been determined experimentally or were estimated based on orthologous enzymes from related species.

3.3.2 Two Substrate Reactions (Irreversible)

The Michaelis–Menten approach to kinetics can be employed even with enzyme reactions that involve two (or more) substrates. In this case it is important to understand the catalytic mechanism. The enzyme 1-deoxy-D-xylulose-5-phosphate (DXP) synthase (*E1* in Fig. 2) is known to utilize an ordered mechanism (substrates bind

in an ordered sequence), with pyruvate (Pyr) binding first and glyceraldehyde 3-phosphate (GAP) second, and then releasing DXP:

$$E1 + Pyr \rightleftharpoons E1 - Pyr \rightleftharpoons E1 - PyrGAP \rightarrow DXP. \quad (5)$$

The following Michaelis–Menten equation is derived:

$$v = \frac{K_{cat} GAP \times [E1_0] \times [Pyr] \times [GAP]}{K_i Pyr \times K_M GAP + K_M Pyr \times [Pyr] + K_M GAP \times [GAP] + [Pyr] \times [GAP]} \quad (6)$$

where K_iPyr is the inhibition constant for pyruvate.

The mechanism of geranyl diphosphate synthase (*E9* in Fig. 2) is unknown and we thus assumed a random order mechanism. The enzyme may bind either substrate (dimethylallyl diphosphate (DMAPP) or isopentenyl diphosphate (IPP)) to produce two possible enzyme–substrate complexes (E9-DMAPP or E9-IPP). This complex then binds the other substrate to form the reactive enzyme complex (E9-DMAPP/IPP or E9-IPP/DMAPP), before releasing the product, geranyl diphosphate (GPP):

$$E9 + DMAPP \rightleftharpoons E9 - DMAPP \rightleftharpoons E9 - DMAPP \,/\, IPP \rightarrow E9 + GPP \quad (7a)$$

$$E9 + IPP \rightleftharpoons E9 - IPP \rightleftharpoons E9 - IPP \,/\, DMAPP \rightarrow E9 + GPP \quad (7b)$$

The initial Michaelis–Menten rate equation (when no product has been formed yet) for enzyme E9 is given by:

$$v = \frac{K_{cat} DMAPP \times [E9_0] \times K_M IPP \times [DMAPP] + K_{cat} IPP \times [E9_0] \times K_M DMAPP \times [IPP]}{K_M IPP \times [IPP] + K_M DMAPP \times [DMAPP] + K_M DMAPP \times K_M IPP} \quad (8)$$

3.3.3 Multiple Product Reactions (Irreversible)

More complex rate equations are used when multiple products need to be considered in the reaction mechanism. Two enzymes of the peppermint monoterpene pathway catalyze reactions that result in the formation of two products from one substrate: (E)-4-hydroxy-3-methyl-but-2-enyl diphosphate reductase (*E7* in Fig. 2) and (+)-pulegone reductase (*E16*). However, since the mechanistic details are unknown, we approximated enzyme behavior by treating the bifurcation as if it was catalyzed by two separate enzymes. Based on previous studies the product ratios of these enzymes were known (*E7* generates 85 % IPP and 15 % DMAPP; *E16* affords 90 % (−)-menthone and 10 % (+)-isomenthone) and we adjusted the enzyme concentrations in the rate equations accordingly (i.e., *E7a* (generating IPP) makes up 85 % and *E7b* (generating DMAPP) accounts for 15 % of the total *E7* concentration). The pathway also contains two enzymes that accept multiple substrates with different affinities: (−)-menthone:(−)-menthol reductase (*E17* in Fig. 2) and (−)-menthone:(+)-neomenthol reductase *E18* in Fig. 2). In these cases we also used a separate equation for each activity (i.e., the equation for *E17a* uses the K_M for (−)-menthone as substrate,

while the equation for *E17b* employs the K_m for (+)-isomenthone as substrate).

3.3.4 Fully Reversible Reactions

The simplest case of a reversible reaction can be outlined as follows:

$$E + S \underset{K_{-1}}{\overset{K_1}{\rightleftharpoons}} ES \underset{K_{-2}}{\overset{K_2}{\rightleftharpoons}} E + P \tag{9}$$

In this case the rate constants of both the forward and reverse reactions need to be considered. Usually, k_1 and k_2 would be summarized as k_f to indicate the rate constant in forward direction, while k_{-1} and k_{-2} would be summarized a k_r to denote the rate constant in reverse direction. The reactions of three enzymes of the peppermint monoterpene pathways had been reported to be reversible: 1-deoxy-D-xylulose 5-phosphate reductoisomerase (*E2* in Fig. 2), isopentenyl diphosphate isomerase (*E8*), and (−)-menthone:(+)-neomenthol reductase ((+)-neomenthol-forming; *E18a*). Using *E2* as an example (1-deoxy-D-xylulose 5-phosphate (DOXP) is the substrate and 2C-methyl-D-erythritol 4-phosphate (ME4P) is the product) the following rate equation is derived for reversible reactions:

$$v = \frac{K_M ME4P \times K_f \times [E2_0] \times [DOXP] - K_M DOXP \times K_r \times [E2_0] \times [ME4P]}{K_M DOXP \times K_r + K_M ME4P \times [DOXP] + K_f \times [ME4P]} \tag{10}$$

3.3.5 Feedback Regulation

In most metabolic networks enzyme activities can be fine-tuned by activation or inhibition. Various kinds of inhibitors, depending on their mode-of-action, have been classified. A thorough treatment of this subject is beyond the scope of this article and the reader is referred to standard text books for details. Two enzymes involved in peppermint monoterpene biosynthesis are known to be affected by competitive feedback inhibition: isopentenyl diphosphate isomerase (*E8*; inbihited by its product geranyl diphosphate) and (+)-pulegone reductase (*E16a*; (−)-menthone-forming activity; uses (+)-pulegone (Pul) as a substrate and is inhibited by the pathway side product (+)-menthofuran (MF)). To account for competitive inhibition the Michaelis–Menten rate equation needs to be modified by including a term containing an experimentally determined inhibition constant (K_i). Using *E16a* as an example, the following rate equation is obtained for inhibition by (+)-menthofuran:

$$\nu = -\frac{K_{cat} Pul \times [E16a_0] \times [Pul]}{[Pul] + K_M Pul \times \left(1 + \frac{[MF]}{K_i MF}\right)} \tag{11}$$

Additionally, *E16a* activity is also affected by inhibition by its substrate, (+)-pulegone:

$$v = -\frac{K_{cat}Pul \times [E16a_0] \times [Pul]}{[Pul] + K_M Pul \times \left(1 + \frac{[Pul]}{K_i Pul}\right)} \quad (12)$$

3.3.6 Other Modeling Assumptions Affecting Kinetic Expressions

In a recent publication [7] we reported that the concentration of (+)-menthofuran was roughly 400 μM in secretory cells obtained from plants grown under greenhouse conditions. Based on the experimentally determined monoterpene profiles of these plants, inhibitory effects on (+)-pulegone reductase were negligible. Our measurements indicated that the concentration of this compound in secretory cells (which is where the enzyme is present) is 100 times less than in the essential oil that accumulates extracellularly in the subcuticular cavity. The expression for competitive inhibition of (+)-pulegone reductase contains the (+)-menthofuran concentration in the denominator (see above). We thus introduced a factor (*z*-factor of 100 for greenhouse growth conditions) to reduce the effect of competitive inhibition on enzyme activity. We also observed that (+)-menthofuran accumulated in secretory cells to high levels under certain adverse environmental conditions [7]. For those cases the *z*-factor is increased accordingly.

A factor "*w*" is used in an analogous fashion to account for the actual concentration of (+)-pulegone in secretory cells. Based on experimental data [7] the concentration of (+)-pulegone in secretory cells is 5 % of the total concentration in glandular trichomes and we thus use a *w*-factor of 0.05 to adjust the (+)-pulegone concentration in the expression for substrate inhibition. It was also observed experimentally that the (+)-pulegone concentration in secretory cells was only marginally affected by environmental conditions and we therefore use a *w*-factor of 0.05 for all simulations.

3.4 Dynamic Developmental Changes in Enzyme Concentrations

For the majority of kinetic mathematical models it is assumed that the amounts of biosynthetic enzymes remain constant for the duration of the experimental period. However, in peppermint glandular trichomes, the biosynthesis of monoterpenes involves dynamic changes in the activities of biosynthetic enzymes [16, 17]. The maximum amount of each enzyme present at the peak of monoterpene biosynthesis (15 days for most enzymes and 20 days for (−)-menthone:(−)-menthol reductase) was determined as described in Subheading 3.2. We thus used the available experimental data on developmental changes in biosynthetic enzyme activities (Fig. 3b) to approximate changes in enzyme amounts with a Gaussian function (Fig. 3c):

$$\frac{\mathrm{d}[E]}{\mathrm{d}t} = Comp \times a \times \mathrm{e}^{\frac{(t-b)^2}{2c^2}} \quad (13)$$

where: Comp = compensation factor to account for the actual concentration of each enzyme in the relevant subcellular environment, a = concentration of enzyme in glandular trichomes (μM) (parameter in the model), t = time (in seconds) after leaf emergence (variable in the model), b = factor defining the center of the Gaussian peak (in seconds) for enzyme activity (parameter in the model), c = factor defining the width of the Gaussian peak (in seconds) for enzyme activity at half maximum (parameter in the model).

To approximate the curve for developmental patterns of enzyme activities with non-Gaussian shapes we used more than one Gaussian function (Fig. 3d).

3.5 Simulating Monoterpene Profiles using MATLAB

Our modeling applies the law of conservation of mass to secretory cells as the reaction volume. We did not perform parameter optimizations as kinetic and other parameters were inferred directly from experimental data. Statistical tests (primarily Chi Square tests) were used to evaluate the goodness of fit of simulated versus experimentally determined monoterpene profiles [8] (note: a description of these statistical methods is not included in this article). We are currently not considering transport processes or thermodynamics.

Our model assumes a limited supply of precursors for monoterpene biosynthesis, pyruvate and glyceraldehyde 3-phosphate ($[S_0]$ = [Pyr] + [GAP] = 1,900 + 1,900 μg per leaf = 3,800 μg per leaf), which is calculated based on the final amount of oil produced by glandular trichomes under various conditions (oil yields are determined experimentally). *See* **Note 1** regarding methods to solve systems of ordinary differential equations (ODEs). To simplify the use of MATLAB for solving a system of ODEs, we are providing a few definitions:

3.5.1 Script File

- A set of commands that includes the vector for pathway metabolites, time span, and the vector of initial conditions.
- It calls the function (m-file) that solves the ODEs and produces the graphical outputs (monoterpene profiles).

3.5.2 Function (m-file)

- Inputs: independent variable t (time span); vector of dependent variables x ([Metabolites]).
- Solves the set of ODEs with the initial values given in the vector of initial conditions. Returns the values of the independent variable in the vector t (time span) and the values of the dependent variables in the vector x ([Metabolites]). The vector of independent variables t is not equally spaced because the function (m-file) controls the step size.

3.5.3 Parameters

- Kinetic constants of enzymes involved in *p*-menthane monoterpene biosynthesis. Not optimized because these values were inferred directly from experimental data.
- *w*-Factor accounts for the small amounts of (+)-pulegone retained in secretory cells (does not change under various environmental conditions). Not optimized because this value was inferred directly from experimental data.
- Reaction volume: volume of secretory cells of glandular trichomes, which was inferred directly from experimental data.

3.5.4 Non-constant Parameters (Variables)

- Independent variable *t* (time span); dependent variable *x* ([Metabolites])
- Gauss function to approximate dynamic changes in enzyme concentrations over time ($d[E]/dt = f(a1 - a18, b1 - b18, c1 - c18)$). Not optimized because the values for parameters *a*, *b*, and *c* were inferred directly from experimental data.
- Logistic function to approximate dynamic changes in the distribution of leaf glandular trichomes over time ($GN = f(a, c, k)$). Not optimized because the values for parameters *a*, *c* and *k* were inferred directly from experimental data. Note that parameters *a* and *c* are not the same as those used for the Gauss function above.
- *z*-Factor accounts for the selective retention of (+)-menthofuran in secretory cells under stress conditions ($z = f$(phenotype, environmental conditions)). Not optimized because this value was inferred directly from experimental data.

In the following paragraphs we are providing a step-by-step guide for the generation of a dynamic kinetic model of peppermint monoterpenoid essential oil biosynthesis. The MATLAB code is provided in its entirety and can be used directly by "cut and paste" from the online version of the article.

1. Open the MATLAB editor.
2. Create a *Script file* with the following commands:
   (a) In the command line write a paragraph describing the MATLAB program (e.g., "Dynamic kinetic model of peppermint essential oil biosynthesis").
   (b) Next, type *Clear* and *clc* for removing all the variables from the workspace, freeing up the system memory, and getting a clean screen.
   (c) Define the vector for pathway metabolites. *See* **Note 2**.
   (d) Define the time interval [$t_{initial}$ to t_{final}] (e.g., tspan = [0 41]). *See* **Note 3**.
   (e) Define the vector for the initial conditions. This is a column vector with values for known initial concentration of

specific intermediate metabolites; the concentration for the remaining metabolites must be set to zero. The vector will have a number of rows equal to the number of metabolites and one column (for wild-type plants grown in the greenhouse use xdot0 = [1900;1900;0;0;0;0;0;0;0;0;0;0;0;0;0;0;0;0;0;0;0;0;0;0;0;0;0;0;0;0;0]). *See* **Note 4**.

(f) Solve the initial value problem for the set of ODE using the ode15s solver. The input arguments to the solver are: *mint_example*, a function that solves the right hand side of the differential equation system; *tspan*, a vector that specifies the interval of integration; *xdot0*, a vector of initial conditions. The output arguments for the solvers are: *t*, a column vector of time points and *x*, a solution array (each row in *x* corresponds to the solution at a time returned in the corresponding row of *t*; e.g., [*t*, *x*] = ode15s (*mint_example*, *tspan*, *xdot0*).

(g) Plot the time course of individual metabolites (e.g., plot (*t*,*x*(:,21)) will generate a plot of the change of metabolite 21 ((−)-menthol) over time).

(h) Save the Script file with an appropriate name e.g., *script_mint_example*. MATLAB commonly saves files in *work*. The complete Matlab code for the Script file is as follows:

```
% Dynamic kinetic model of peppermint essential oil
  biosynthesis

% Metabolite Nomenclature

%[GAP]      D-Glyceraldehyde 3-Phosphate
%[Pyr]      Pyruvate
%[DOXP]     1-Deoxy-D-xylulose 5-phosphate
%[ME4P]     2-C-Methyl-D-erythritol-4-phosphate
%[CDPME]    4-(Cytidine  5'-diphospho)-2-C-methyl-D-
            erythritol
%[CDPME2P]  2-Phospho-4-(cytidine5'-diphospho)-2-C-methyl-D-
            erythritol
%[MEcPP]    2-C-Methyl-D-erythritol-2,4-
            cyclodiphosphate
%[HMBPP]    1-Hydroxy-2-methyl-2-(E)-butenyl
            4-diphosphate
%[DMAPP]    Dimethylallyl diphosphate
%[IPP]      Isopentenyl diphosphate
%[GPP]      Geranyl diphosphate
%[LIM]      (-)-Limonene
%[IPPol]    (-)-trans-Isopiperitenol
%[IPPone]   (-)-Isopiperitenone
%[CIPUL]    (+)-cis-Isopulegone
%[PUL]      (+)-Pulegone
%[MF]       (+)-Menthofuran
%[IMone]    (+)-Isomenthone
%[Mone]     (-)-Menthone
```

```
%[NMol]     (+)-Neomenthol
%[Mol]      (-)-Menthol
%[IMol]     (+)-Isomenthol
%[NIMol]    (+)-Neoisomenthol

clear all
clc

%Vector for pathway metabolites
Xdot = zeros(23,1);

%Time interval
Tspan = [0 3456000]; % [sec] (equivalent to 41 days)

%vector for initial conditions
xdot0 = [1900;1900;0;0;0;0;0;0;0;0;0;0;0;0;0;0;0;0;0;0;
        0;0;0;0;0];

% solving the initial value problem

[t,x] = ode15s('mint_example', tspan, xdot0, []);

GAP = x(:,1);
Pyr = x(:,2);
DOXP = x(:,3);
MEP4 = x(:,4);
CDPME = x(:,5);
CDPME2P = x(:,6);
MEcPP = x(:,7);
HMBPP = x(:,8);
DMAPP = x(:,9);
IPP = x(:,10);
GPP = x(:,11);
LIM = x(:,12);
IPPol = x(:,13);
IPPone = x(:,14);
CIPUL = x(:,15);
PUL = x(:,16);
MF = x(:,17);
IMone = x(:,18);
Mone = x(:,19);
NMol = x(:,20);
Mol = x(:,21);
IMol = x(:,22);
NIMol = x(:,23);

% Plotting

plot(t/86400,PUL,'b',t/86400,MF,'g',t/86400,Mone,'c',
t/86400,Mol,'r')

Legend('PUL','MF','Mone','Mol')
Title('Monoterpene Accumulation in Secretory cells')
xlabel('Time (day)')
ylabel('Monoterpene Concentration ')
Axis([0 40 - 20 1000])
```

3. Create the mint_example function that solves the ODE system. In the MATLAB editor click the New M-file tab:
   (a) Type the command function into the command line, followed by the name of the column vector containing the left hand side of the ODE system, equaled to the function name and its arguments (e.g., function xdot = mint_example (t,x)). Note the name of the function must match the function name in the command line for the solution of the initial value problem in 2f.
   (b) In the command line write a paragraph describing the MATLAB program (e.g., "This function calculates monoterpene amounts (41 day time course) in leaves of peppermint WT plants grown in a greenhouse with supplemental lighting from sodium vapor lights").
   (c) Define all parameters and inhibition and kinetic constants drawn in the rate of reaction equations.
   (d) Write the ODE system in matrix notation. The left hand side will be a column vector with dimensions, number of mass balances (metabolites) times 1. The right hand side will be a column vector whose elements will be mass balances for each intermediate metabolite; e.g., xdot = [$R_{\text{production of metabolite 1}} - R_{\text{consumption of metabolite 1}}$; $R_{\text{production of metabolite 2}} - R_{\text{consumption of metabolite 2}}$; $R_{\text{production of metabolite 3}} - R_{\text{consumption of metabolite 3}}$;], and so on.
   (e) Save the M-file as mint_example in the MATLAB WORK file.

```
function xdot = mint_example(t,x)
% This function calculates monoterpene amounts (41
  day time course) in leaves
% of peppermint WT plants grown in a greenhouse with
  supplemental lighting from sodium vapor lights.
% A mechanism following regular Michaelis-Menten-
  type kinetics is assumed for all enzymes with the
  following exceptions:
% (1) Substrate inhibition of (+)-pulegone reductase
% (2) Competitive inhibition of (+)-pulegone reduc-
  tase by (+)-menthofuran
% (3) Competitive inhibition of isopentenyl-diphoshate
  isomerase by GPP
% (4) Reversible reaction mechanisms were assume for
  1-Deoxy-D-xylulose-5-phosphate reductoisomerase
  and (-)-Menthone:(+)-neomenthol reductase
% (5) Bi-bi (two substrates, two products) reaction
  mechanisms were assumed for 1-deoxy-D-xylulose-
  5-phosphate synthase (Pyruvate+GAP = DXP+Co2) and
  geranyl diphosphate synthase (IPP+DMAPP = GPP+PPi).
  The former utilizes an ordered mechanism (Pyr binds
  first), whereas a random mechanism is assumed for
  the latter.
```

```
% Metabolite Nomenclature
%[GAP]      D-Glyceraldehyde 3-Phosphate
%[Pyr]      Pyruvate
%[DOXP]     1-Deoxy-D-xylulose 5-phosphate
%[ME4P]     2-C-Methyl-D-erythritol-4-phosphate
%[CDPME]    4-(Cytidine  5'-diphospho)-2-C-methyl-D-
            erythritol
%[CDPME2P]  2-Phospho-4-(cytidine
            5'-diphospho)-2-C-methyl-D-erythritol
%[MEcPP]    2-C-Methyl-D-erythritol-2,
            4-cyclodiphosphate
%[HMBPP]    1-Hydroxy-2-methyl-2-(E)-butenyl
            4-diphosphate
%[DMAPP]    Dimethylallyl diphosphate
%[IPP]      Isopentenyl diphosphate
%[GPP]      Geranyl diphosphate
%[LIM]      (-)-Limonene
%[IPPol]    (-)-trans-Isopiperitenol
%[IPPone]   (-)-Isopiperitenone
%[CIPUL]    (+)-cis-Isopulegone
%[PUL]      (+)-Pulegone
%[MF]       (+)-Menthofuran
%[IMone]    (+)-Isomenthone
%[Mone]     (-)-Menthone
%[NMol]     (+)-Neomenthol
%[Mol]      (-)-Menthol
%[IMol]     (+)-Isomenthol
%[NIMol]    (+)-Neoisomenthol

% Kinetic Parameters

% kc units: [1/s] kc = Kcat
% KM units: [uM]
% Ki units: [uM]

KM1a = 68;   %1-Deoxy-D-xylulose-5-phosphate synthase
             (DXS) for GAP
kc1a = 1.9;
KM1b = 440;  %1-Deoxy-D-xylulose-5-phosphate synthase
             (DXS) for Pyr
kc1b = 1.9;
Kia = 16;    %Dissociation constant for Pyr
KM2f = 132;  %1-Deoxy-D-xylulose-5-phosphate   reducto
             isomerase (DXR; forward reaction)
kc2f = 4.4;
KM2r = 972;  %1-Deoxy-D-xylulose-5-phosphate   reducto
             isomerase (DXR; reverse reaction)
kc2r = 1.6;
KM3 = 500;   %2-C-Methyl-D-erythritol    4-phosphate
             cytidylyltransferase (MCT)
kc3 = 26;
KM4 = 100;   %4-(Cytidine  5'-diphospho)-2-C-methyl-
             D-erythritol kinase (CMK)
```

```
kc4 = 1;
KM5 = 252;   %2-C-Methyl-D-erythritol      2,4-cyclo
             diphosphate synthase (MECPS)
kc5 = 1;
KM6 = 420;   %4-Hydroxy-3-methylbut-2-en-1-yl
             diphosphate synthase (HDS)
kc6 = 0.4;
KM7 = 30;    %4-Hydroxy-3-methylbut-2-en-1-yl
             diphosphate reductase (HDR)
kc7 = 3.7;
KM8f = 5.1;  %Isopentenyl-diphosphate   delta-isomer
             ase for IPP (IPPI; forward reaction)
kc8f  = 0.018;
KM8r = 17;   %Isopentenyl-diphosphate   delta-isomer
             ase for DMAPP (IPPI; rev reaction)
kc8r = 0.89;
KM9a = 54;   %Geranyl  diphosphate  synthase  (GPPS;
             DMAPP as substrate)
kc9a = 48;
KM9b = 26;   %Geranyl  diphosphate  synthase  (GPPS;
             IPP as substrate)
kc9b = 48;
KM10 = 20;   %(-)-Limonene synthase (LS)
kc10 = 0.3;
KM11 = 18;   %(-)-Limonene 3-hyroxylase (L3H)
kc11 = 1;
KM12 = 72;   %(-)-trans-Isopiperitenol dehydrogenase
             (IsoDH)
kc12 = 0.002;
KM13 = 1;    %(-)-Isopiperitenone reductase (IsoR)
kc13 = 1.3;
KM14 = 270;  %(+)-cis-Isopulegone isomerase (IsoI)
kc14 = 1;
KM15 = 10;   %(+)-Menthofuran synthase (MFS)
kc15 = 0.9;
KM16a = 2.3; %(+)-Pulegone  reductase  (PR;  product:
             (-)-menthone)
kc16a = 1.8;
KM16b = 2.3; %(+)-Pulegone  reductase  (PR;  product:
             (+)-isomenthone)
kc16b = 1.8;
KM17a = 3;   %(-)-Menthone:(-)-menthol     reductase
             (MMR; substrate: (-)-menthone)
kc17a = 0.6;
KM17b = 41;  %(-)-Menthone:(-)-menthol     reductase
             (MMR; substrate: (+)-isomenthone)
kc17b = 0.6;
KM18af = 674; %(-)-Menthone:(+)-neomenthol   reductase
              (MNR; substrate: (-)-menthone); forward
              reaction)
kc18af = 0.06;
```

```
KM18ar = 1200; %(-)-Menthone:(+)-neomenthol reductase (MNR; substrate: (-)-menthone); (backward reaction)
kc18ar = 0.06;% estimated
KM18b = 1000; %(-)-Menthone:(+)-neomenthol reductase (MNR; substrate: (+)-isomenthone)
kc18b = 0.06;

Kic1 = 96; % Product inhibition constant (Geranyl diphosphate acting on IPPI)
Kic2 = 300; % Product inhibition constant ((+)-menthofuran acting on PR)
% Competitive inhibition mechanism

Kis = 112; % Substrate Inhibition constant ((+)-pulegone acting on PR)
% Uncompetitive inhibition mechanism

Z = 100; % Factor to account for selective retention of (+)-menthofuran in secretory cells

W = 0.05; % Factor to account for the rapid excretion of (+)-pulegone from secretory cells into oil storage cavity

% The model also takes into account that each enzyme shows a particular transient pattern of expression. This pattern is approximated by a Gauss function.

%First peak of activity:

%f(x) = Comp * a * exp((-(t-b).^2)/(2*(c)^2))

%where Comp = Factor to adjust for the volume density of the compartment in which a particular enzyme is active [Dimensionless]
% a = Factor defining the height of the Gaussian peak for enzyme activity [ Units of concentration ]
% t = Time [s]
% b = Factor defining the position of the center of the Gaussian peak for enzyme activity [s]
% c = Factor defining the width of the Gaussian peak for enzyme activity at half maximum [s]

b1 = 1296000; % Defines the position of the center of the Gaussian peak for enzyme activity. Relevant to the following enzyme activities: LS, L3H, IsoDH, IsoR, IsoI, MFS, PR
c1 = 800000; % Defines the width of the Gaussian peak for enzyme activity at half maximum. Relevant to the following enzyme activities: LS, L3H, IsoDH, IsoR, IsoI, MFS, PR

b5 = 1800000; % Defines the position of the center of the Gaussian peak for enzyme activity. Relevant to the following enzyme activities: MMR, MNR

c5 = 900000; % Defines the width of the Gaussian peak for enzyme activity at half maximum. Relevant to the following enzyme activities: MMR, MNR

E1 = (0.139)*1*exp((-(t-b1).^2)/(2*(c1)^2));% DXS
```

```
E2 = (0.139)*1*exp((-(t-b1).^2)/(2*(c1)^2)); % DXR
E3 = (0.139)*1.2*exp((-(t-b1).^2)/(2*(c1)^2)); % MCT
E4 = (0.139)*1*exp((-(t-b1).^2)/(2*(c1)^2)); % CMK
E5 = (0.139)*1.2*exp((-(t-b1).^2)/(2*(c1)^2)); % MECPS
E6 = (0.139)*1.2*exp((-(t-b1).^2)/(2*(c1)^2)); % HDS
E7a = (0.139)*2*exp((-(t-b1).^2)/(2*(c1)^2)); % HDR
      (product: DMAPP)
E7b = (0.139)*0.4*exp((-(t-b1).^2)/(2*(c1)^2)); % HDR
      (product: IPP)
E8 = (0.139)*1.4*exp((-(t-b1).^2)/(2*(c1)^2)); % IPPI
E9 = (0.139)*1*exp((-(t-b1).^2)/(2*(c1)^2)); % GPPS
E10 = (0.139)*1.1*exp((-(t-b1).^2)/(2*(c1)^2)); % LS
E11 = (0.365)*1*exp((-(t-b1).^2)/(2*(c1)^2)); % L3H
E12 = (0.044)*13.6*exp((-(t-b1).^2)/(2*(c1)^2)); % IsoDH
E13 = (0.204)*1.2*exp((-(t-b1).^2)/((2*c1)^2)); % IsoR
E14 = (0.204)*1.2*exp((-(t-b1).^2)/((2*c1)^2)); % IsoI
E15 = (0.365)*0.00012*exp((-(t-b1).^2)/(2*(c1)^2));
      % MFS
E16a = (0.204)*0.003*exp((-(t-b1).^2)/(2*(c1)^2));
       % PR (product: (-)-menthone)
E16b = (0.204)*0.0003*exp((-(t-b1).^2)/(2*(c1)^2));
       % PR (product: (+)-isomenthone)
E17a = (0.204)*0.0023*exp((-(t-b5).^2)/(2*(c5)^2));
       % MMR (product: (-)-menthol)
E17b = (0.204)*0.0023*exp((-(t-b5).^2)/(2*(c5)^2));
       % MMR (product: (+)-neoisomenthol)
E18a = (0.204)*0.00001*exp((-(t-b5).^2)/(2*(c5)^2));
       % MNR (product: (+)-neomenthol)
E18b = (0.204)*0.00001*exp((-(t-b5).^2)/(2*(c5)^2));
       % MNR (product: (+)-isomenthol)

% The model also takes into account that the glandular
trichome density (GN) changes over time. This behavior
is approximated using a logistic function:

c = 8*10^4;  % parameter approximating slope of
exponential phase of sigmoid curve
k = 1/9*10^4; % parameter approximating shape of sigmoid
curve

GN = (1/(1+c*exp(-k*t))); % at day 15, gland number
is 86.7 % of total gland number at day 30
%Species Equations
xdot = [GN*(-(kc1b*E1*x(2)*x(1)/(Kia*KM1b+KM1a*x(2)+
KM1b*x(1)+x(1)*x(2)))); % Variation of GAP
GN*(-(kc1b*E1*x(2)*x(1)/(Kia*KM1b+KM1a*x(2)+KM1b*x
(1)+x(1)*x(2)))); % Variation of Pyruvate (same
expression as for GAP)
GN*((kc1b*E1*x(2)*x(1)/(Kia*KM1b+KM1a*x(2)+KM1b*x(1)
+x(1)*x(2)))-((KM2r*kc2f*E2*x(3)-KM2f*kc2r*E2*x(4))/
(KM2f*KM2r+KM2r*x(3)+KM2f*x(4)))); % Variation of
DOXP
GN*(((KM2r*kc2f*E2*x(3)-KM2f*kc2r*E2*x(4))/
(KM2f*KM2r+KM2r*x(3)+KM2f*x(4)))-(kc3*E3*x(4)/
(x(4)+KM3))); % Variation of ME4P
```

```
GN*((kc3*E3*x(4)/(x(4)+KM3))-(kc4*E4*x(5)/
(x(5)+KM4))); % Variation of CDP-ME
GN*((kc4*E4*x(5)/(x(5)+KM4))-(kc5*E5*x(6)/
(x(6)+KM5))); % Variation of CDP-ME2P
GN*((kc5*E5*x(6)/(x(6)+KM5))-(kc6*E6*x(7)/(x(7)+KM6)));
 % Variation of MEcPP
GN*((kc6*E6*x(7)/(x(7)+KM6))-(kc7*E7a*x(8)/
(x(8)+KM7))- (kc7*E7b*x(8)/(x(8)+KM7))); % Variation
of HMB-PP
GN*((kc7*E7a*x(8)/(x(8)+KM7))+(kc8f*E8*x(10)/(x(10)
+KM8f*(1+(x(11)/Kic1))))-(kc8r*E8*x(9)/(x(9)
+KM8r*(1+(x(11)/Kic1))))-((kc9a*E9*KM9b*x(9)
+kc9b*E9*KM9a*x(10))/(KM9b*x(9)+KM9a*x(10)+KM9a*K
M9b))); %Variation of DMAPP
GN*((kc7*E7b*x(8)/(x(8)+KM7))+(kc8r*E8*x(9)/(x(9)
+KM8r*(1+(x(11)/Kic1))))-(kc8f*E8*x(10)/(x(10)
+KM8f*(1+(x(11)/Kic1))))-((kc9a*E9*KM9b*x(9)
+kc9b*E9*KM9a*x(10))/(KM9b*x(9)+KM9a*x(10)+KM9a*K
M9b))); %Variation of IPP
GN*(((kc9a*E9*KM9b*x(9)+kc9b*E9*KM9a*x(10))/(KM9b*x(9)
+KM9a*x(10)+KM9a*KM9b))- (kc10*E10*x(11)/(x(11)+KM10)));
 %Variation of GPP
GN*((kc10*E10*x(11)/(x(11)+KM10))-(kc11*E11*x(12)/
(x(12)+KM11))); % Variation of LIM
GN*((kc11*E11*x(12)/(x(12)+KM11))-(kc12*E12*x(13)/
(x(13)+KM12))); % Variation of IPPol
GN*((kc12*E12*x(13)/(x(13)+KM12))-(kc13*E13*x(14)/
(x(14)+KM13))); % Variation of IPPone
GN*((kc13*E13*x(14)/(x(14)+KM13))-(kc14*E14*x(15)/
(x(15)+KM14))); % Variation of CIPUL
GN*((kc14*E14*x(15)/(x(15)+KM14))-(kc16a*E16a*
x(16)/(x(16)+KM16a*(1+z*(x(17))/Kic2)))-(kc16b*E16b*
x(16)/(x(16)+KM16b*(1+z*(x(17))/Kic2)))-(w*kc16a*
E16a*x(16)/(KM16a+x(16)*(1+x(16)/Kis)))-(w*kc16b*
E16b*x(16)/(KM16b+x(16)*(1+x(16)/Kis)))-(kc15*E15
*x(16)/(x(16)+KM15))); % Variation of PUL
GN*(kc15*E15*x(16)/(x(16)+KM15)); % Variation of MF
GN*((kc16b*E16b*x(16)/(x(16)+KM16b*(1+z*(x(17))/Kic2)))
+(w*kc16b*E16b*x(16)/(KM16b+x(16)*(1+x(16)/Kis)))-
(kc17b*E17b*x(18)/(x(18)+KM17b))-(kc18b*E18b*x(18)/
(x(18)+KM18b))); % Variation of IMone
GN*((kc16a*E16a*x(16)/(x(16)+KM16a*(1+z*(x(17))/
Kic2)))+(w*kc16a*E16a*x(16)/(KM16a+x(16)*(1+x(16)/
Kis)))-((KM18ar*kc18af*E18a*x(19)-
KM18af*kc18ar*E18a*x(20))/(KM18af*KM18ar+KM18ar*x(1
9)+KM18af*x(20)))-(kc17a*E17a*x(19)/
(x(19)+KM17a))); % Variation of Mone
GN*((KM18ar*kc18af*E18a*x(19)-KM18af*kc18ar*
E18a*x(20))/(KM18af*KM18ar+KM18ar*x(19)+KM18a
f*x(20))); % Variation of NMol
GN*(kc17a*E17a*x(19)/(x(19)+KM17a)); % Variation of Mol
GN*(kc18b*E18b*x(18)/(x(18)+KM18b)); % Variation of IMol
```

```
GN*(kc17b*E17b*x(18)/(x(18)+KM17b))]; % Variation of
NIMol
```

Now that both a script file and an M-file have been generated, a simulation can be plotted in MATLAB:

4. Start MATLAB
5. Click on File, Open and choose the corresponding script file script_mint_example. The MATLAB editor will display the code.
6. Click on Debug and select Run for running the script. Alternatively, typing F5 will also run the program. If all the parameters and kinetic constants integrated in the reaction rate equations have been defined in the M-file, the program will plot the time course variation for the selected intermediate metabolites. The Matlab code will include the command plot followed by time (all the elements in the vector t), and the name of the metabolite to be plotted (specific element in the vector x). Matlab will automatically display the corresponding curve in a default color, although color preferences can be adjusted. For example, the command:

```
plot(t/86400,PUL,'b',t/86400,MF,'g',t/86400,Mone,'r')
```

will plot the changes in the amounts of the metabolites (+)-pulegone, (+)-menthofuran, and (−)-menthone in blue, green, and red, respectively (the time domain is a day, which consists of 86,400 s, the time unit used in the code). Make sure to save all files if you should decide to change code or commands.

4 Notes

1. One option for solving a system of ordinary differential equations (ODEs) in the MATLAB® framework (http://www.mathworks.com/products/matlab) is the *ode45* solver, which uses the Runge–Kutta higher order method. However, this method does not work well with stiff differential equations [18]. In such cases, the ode15s solver is recommended.
2. In the example in Subheading 3.5, the vector for pathway metabolites must be a column vector with zeros as elements; it will have a number of rows equal to the number of metabolites and one column, for example:

   ```
   Xdot = zeros (23,1)
   ```

3. Note that the plot in the example in Subheading 3.5 uses days as the time unit as this is more convenient than the unit used for modeling (seconds).
4. In the example in Subheading 3.5, the units for concentration must match those for the rate of reaction.

Acknowledgements

This work was funded by a grant from the Energy Biosciences Division of the US Department of Energy (DE-FG02-09ER16054).

References

1. Tomita M, Hashimoto K, Takahashi K et al (1999) ECELL: software environment for whole-cell simulation. Bioinformatics 15:72–84
2. Rios-Estepa R, Lange BM (2007) Experimental and mathematical approaches to modeling plant metabolic networks. Phytochemistry 68:2351–2374
3. Resat H, Petzold L, Pettigrew MF (2009) Kinetic modeling of biological systems. Methods Mol Biol 541:311–335
4. Schallau K, Junker B (2010) Simulating plant metabolic pathways with enzyme-kinetic models. Plant Physiol 152:1763–1771
5. Van Riel NAW (2006) Dynamic modelling and analysis of biochemical networks: mechanism-based models and model-based experiments. Brief Bioinform 7:364–374
6. Schwender J (2009) Kinetic properties of metabolic networks. In: Schwender J (ed) Plant metabolic networks. Springer, New York, pp 307–322
7. Rios-Estepa R, Turner GW, Lee JM, Croteau RB, Lange BM (2008) A systems biology approach identifies the biochemical mechanisms regulating monoterpenoid essential oil composition in peppermint. Proc Natl Acad Sci U S A 105:2818–2823
8. Rios-Estepa R, Lange I, Lee JM, Lange BM (2010) Mathematical modeling-guided evaluation of biochemical, developmental, environmental, and genotypic determinants of essential oil composition and yield in peppermint leaves. Plant Physiol 152:2105–2119
9. Croteau R, Davis EM, Ringer KL, Wildung MR (2005) (−)-Menthol biosynthesis and molecular genetics. Naturwiss 92:562–577
10. Ringer KL, McConkey ME, Davis EM, Rushing GW, Croteau R (2003) Monoterpene double-bond reductases of the (−)-menthol biosynthetic pathway: isolation and characterization of cDNAs encoding (−)-isopiperitenone reductase and (+)-pulegone reductase of peppermint. Arch Biochem Biophys 418:80–92
11. Turner GW, Gershenzon J, Croteau R (2000) Development of peltate glandular trichomes of peppermint (*Mentha × piperita* L.). Plant Physiol 124:655–664
12. Turner GW, Gershenzon J, Nielson EE, Froehlich JE, Croteau R (1999) Limonene synthase, the enzyme responsible for monoterpene biosynthesis in peppermint, is localized to leucoplasts of oil gland secretory cells. Plant Physiol 120:879
13. Bertea CM, Schalk M, Karp F, Maffei M, Croteau R (2001) Demonstration that menthofuran synthase of mint (Mentha) is a cytochrome P450 monooxygenase: cloning, functional expression, and characterization of the responsible gene. Arch Biochem Biophys 390:279–286
14. Turner GW, Croteau R (2004) Organization of monoterpene biosynthesis in Mentha. Immunocytochemical localizations of geranyl diphosphate synthase, limonene-6-hydroxylase, isopiperitenol dehydrogenase, and pulegone reductase. Plant Physiol 136:4215
15. Fersht A (1985) Structure and mechanism in protein science. W.H. Freeman and Company, New York. ISBN 0716732688
16. Gershenzon J, McConkey ME, Croteau RB (2000) Regulation of monoterpene accumulation in leaves of peppermint. Plant Physiol 122:205–214
17. McConkey ME, Gershenzon J, Croteau RB (2000) Developmental regulation of monoterpene biosynthesis in the glandular trichomes of peppermint. Plant Physiol 122:215–224
18. Harman TL, Dabney J, Richert N (2000) Advanced engineering mathematics with MATLAB. Brooks/Cole Publishing Co, Pacific Grove. ISBN 0534371647
19. Lange BM, Wildung MR, McCaskill D, Croteau R (1998) A family of transketolases that directs isoprenoid biosynthesis via a mevalonate-independent pathway. Proc Natl Acad Sci U S A 95:2100–2104
20. Eubanks LM, Poulter CD (2003) Rhodobacter capsulatus 1-deoxy-D-xylulose 5-phosphate synthase: steady-state kinetics and substrate binding. Biochemistry 42:1140–1149
21. Lange BM, Croteau R (1999) Isoprenoid biosynthesis via a mevalonate-independent pathway in plants: cloning and heterologous expression of 1-deoxyxylulose-5-phosphate

reductoisomerase from peppermint. Arch Biochem Biophys 365:170–174

22. Rohdich F, Lauw S, Kaiser J et al (2006) Isoprenoid biosynthesis in plants – 2C-methyl-D-erythritol-4-phosphate synthase (IspC protein) of Arabidopsis thaliana. FEBS J 273:4446–4458
23. Rohdich F, Wungsintaweekul J, Eisenreich W et al (2000) Biosynthesis of terpenoids: 4-diphosphocytidyl-2C-methyl-D-erythritol synthase of Arabidopsis thaliana. Proc Natl Acad Sci U S A 97:6451–6456
24. Lange BM, Croteau R (1999) Isopentenyl diphosphate biosynthesis via a mevalonate-independent pathway: isopentenyl monophosphate kinase catalyzes the terminal enzymatic step. Proc Natl Acad Sci U S A 96:13714–13719
25. Rohdich F, Wungsintaweekul J, Lüttgen H et al (2000) Biosynthesis of terpenoids: 4-diphosphocytidyl-2-C-methyl-D-erythritol kinase from tomato. Proc Natl Acad Sci U S A 97:8251–8256
26. Bernal C, Mendez E, Terencio J, Boronat A, Imperial S (2005) A spectrophotometric assay for the determination of 4-diphosphocytidyl-2-C-methyl-D-erythritol kinase activity. Anal Biochem 250:245–251
27. Gao S, Lin J, Liu X et al (2006) Molecular cloning, characterization and functional analysis of a 2C-methyl-D-erythritol 2, 4-cyclodiphosphate synthase gene from Ginkgo biloba. J Biochem Mol Biol 39:502–510
28. Rohdich F, Eisenreich W, Wungsintaweekul J et al (2001) Biosynthesis of terpenoids. 2C-Methyl-D-erythritol 2,4-cyclodiphosphate synthase (IspF) from Plasmodium falciparum. Eur J Biochem 268:3190–3197
29. Shi W, Feng J, Zhang M et al (2007) Biosynthesis of isoprenoids: characterization of a functionally active recombinant 2-C-methyl-D-erythritol 4-phosphate cytidyltransferase (IspD) from Mycobacterium tuberculosis H37Rv. Biochem Mol Biol 40:911–920
30. Querol J, Campos N, Imperial S, Boronat A, Rodríguez-Concepción M (2002) Functional analysis of the Arabidopsis thaliana GCPE protein involved in plastid isoprenoid biosynthesis. FEBS Lett 514:343–346
31. Kollas AK, Duin EC, Eberl M et al (2002) Functional characterization of GcpE, an essential enzyme of the non-mevalonate pathway of isoprenoid biosynthesis. FEBS Lett 532:432–436
32. Hsieh MH, Goodman HM (2005) The Arabidopsis IspH homolog is involved in the plastid nonmevalonate pathway of isoprenoid biosynthesis. Plant Physiol 138:641–653
33. Altincicek B, Duin EC, Reichenberg A et al (2002) LytB protein catalyzes the terminal step of the 2-C-methyl-erythritol-4-phosphate pathway of isoprenoid biosynthesis. FEBS Lett 532:437–440
34. Graewert T, Kaiser J, Zepeck F et al (2004) IspH protein of Escherichia coli: studies on iron–sulfur cluster implementation and catalysis. J Am Chem Soc 126:12847–12855
35. Ramos-Valdivia AC, van der Heijden R, Verpoorte R, Camara B (1997) Purification and characterization of two isoforms of isopentenyl-diphosphate isomerase from elicitor-treated Cinchona robusta cells. Eur J Biochem 249:161–170
36. Burke C, Croteau R (2002) Geranyl diphosphate synthase from Abies grandis: cDNA isolation, functional expression, and characterization. Arch Biochem Biophys 405:130–136
37. Alonso WR, Rajaonarivony JI, Gershenzon J, Croteau R (1992) Purification of 4S-limonene synthase, a monoterpene cyclase from the glandular trichomes of peppermint (Mentha×piperita) and spearmint (Mentha spicata). J Biol Chem 267:7582–7587
38. Karp F, Mihaliak CA, Harris JL, Croteau R (1990) Monoterpene biosynthesis: specificity of the hydroxylations of (–)-limonene by enzyme preparations from peppermint (Mentha piperita), spearmint (Mentha spicata), and perilla (Perilla frutescens) leaves. Arch Biochem Biophys 276:219–226
39. Ringer KL, Davis EE, Croteau R (2005) Monoterpene metabolism. Cloning, expression, and characterization of (–)-Isopiperitenol/(–)-carveol dehydrogenase of peppermint and spearmint. Plant Physiol 137:863–872
40. Kjonaas R, Martinkus-Taylor C, Croteau R (1982) Metabolism of monoterpenes: conversion of L-menthone to L-menthol and D-neomenthol by stereospecific dehydrogenases from peppermint (Mentha piperita) leaves. Plant Physiol 69:1013–1017
41. Davis EE, Ringer KL, McConkey ME, Croteau R (2005) Monoterpene metabolism. Cloning, expression, and characterization of menthone reductases from peppermint. Plant Physiol 137:873–881